

pubs.acs.org/journal/ascecg Research Article

# Acid-Modified, Ti<sub>3</sub>C<sub>2</sub>-Based MXene as Catalysts for Upcycling Polyethylene Terephthalate

Iuliana M. Chirica, Anca G. Mirea, Tudor Şuteu, Andrei Kuncser, Ştefan Neaţu, Mihaela Florea, Michel W. Barsoum, and Florentina Neaţu\*



Cite This: ACS Sustainable Chem. Eng. 2024, 12, 9766-9776



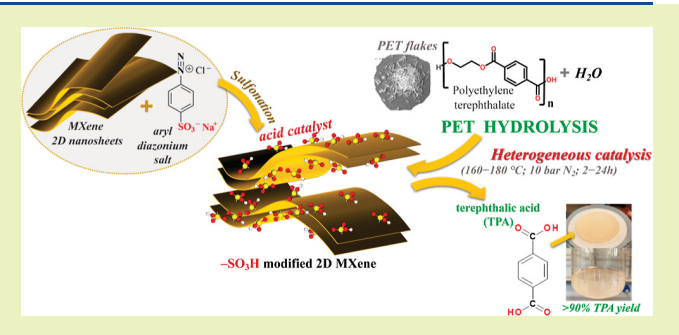
**ACCESS** 

III Metrics & More

Article Recommendations

Supporting Information

**ABSTRACT:** Plastics are indispensable materials for packaging and many products from our daily life, and their recycling is essential to ensure a circular economy. In this study,  $-SO_3H$ -modified,  $Ti_3C_2$ -MXene was used as a recoverable solid acid catalyst for upcycling of polyethylene terephthalate (PET) to terephthalic acid (TPA) and ethylene glycol by hydrolysis. For the grafting of  $-SO_3H$  groups to the  $Ti_3C_2T_x$  surface (where  $T_x$  represents the surface moieties, such as -OH or -O), sulfonation with an aryl diazonium salt obtained from sulfanilic acid was employed. X-ray photoelectron and Fourier transform infrared spectroscopy analyses provided a direct indication that sulfonation



of the  $Ti_3C_2T_x$  was successfully performed, while X-ray diffraction and transmission electron microscopy analyses evidence the presence of  $-SO_3H$  groups between the  $Ti_3C_2T_x$  layers due to the increases of the interlayer spacing through the intercalation of functional groups. The higher the concentration of acid groups, the higher the interlayer spacing. The depolymerization of PET in water occurred with a very good isolated yield in TPA (99%) for the MXene with the highest amount of sulfonic acid groups. We conclude that the acidity is mandatory to perform the hydrolysis reaction, in agreement with the acidity measurements, which show that the MXenes modified with the highest amount of derived sulfonic acids are the most active. Nevertheless, the accessibility to the acidic sites is a key factor that promotes the 2D acid-modified MXene materials as important catalysts for PET upcycling to TPA.

KEYWORDS: PET, depolymerization, MXene, sulfonation, hydrolysis

#### **■** INTRODUCTION

One of the biggest challenges today is related to the paradigm of a highly endangered ecological system in contrast to the economic and social expansion that humanity has experienced in the last century. The prosperity of developing countries brings a much greater global consumption of energy, which mankind does not yet know how to manage, and which has an extraordinary impact on global warming.1 Keeping the situation under control is usually addressed by government regulations and happens locally. Reaching the targets set by legislation is what forces us to limit, or find solutions, to curb energy consumption.<sup>2</sup> One of the main solutions is related to a circular economy in all areas. For the oil industry, which remains the main source of polymers at the present time, this circular economy means collecting and recirculating carbon products. One of the most widespread resources of used carbon is plastic, and its recycling is becoming more and more imperative. Incineration accounts for 25% of plastic reuse, followed by mechanical recycling (12%); only  $\approx$ 1% is returned to monomer form.<sup>3</sup>

One of the most widely used plastics on the global market remains poly(ethylene terephthalate) (PET), due to its versatility and ease of use. Its utilization has continuously increased over the years, resulting in significant waste generation, which therefore requires improved recycling rates. Mechanical recycling routes of PETs are limited by the fact that only clean PET can be recycled and also because the latter is characterized by lower thermal, optical, and mechanical properties than the pristine material. Chemical recycling into monomers remains an advantageous alternative compared to other methods because lower molecular weight products can more easily re-enter in the PET polymerization process and can also be converted into other compounds with added chemical value, which can be used in various fields.

Until recently, most of chemical recycling processes have mainly focused on pyrolysis and solvolysis, and there are several reviews on this topic.<sup>6–8</sup> As a result of legislative pressure, catalytic recycling processes have developed greatly and have experienced rapid growth in recent years.<sup>5</sup> Thus,

Received: March 6, 2024 Revised: June 4, 2024 Accepted: June 5, 2024 Published: June 14, 2024





Scheme 1. Schematic Representation of MXene Sulfonation



hydrogenolysis,  $^{9-13}$  aminolysis,  $^{14,15}$  hydrosilylation,  $^{16,17}$  and photocatalysis  $^{18,19}$  have gained much ground to recycle plastics. However, in the chemical recycling of PET, some issues still need to be solved such as the generation of undesired byproducts, the use of large amounts of solvents, high costs in the separation and purification of reaction product mixtures, and energy consumption in the form of the need for high temperatures. In the case of homogeneous catalytic processes, the separation of the catalyst from the reaction mixture is a problem.<sup>20</sup> Among the chemical methods involving the use of a solvent (i.e., glycolysis, methanolysis, aminolysis, or hydrolysis), glycolysis is one of the most studied, while hydrolysis is the most cost-efficient because it produces the initial monomers ethylene glycol (EG) and terephthalic acid (TPA). However, the hydrolysis process is challenging due to the fact that it requires high working temperatures (200-250 °C) and pressures (1.4-2 MPa) as well as long reaction times to achieve complete depolymerization. Consequently, finding a heterogeneous, stable, and inexpensive catalyst that leads to high TPA yields by hydrolysis and works at relatively low temperatures and pressures fits better with the idea of circular economy.

The strategy of this study is to develop an acidic heterogeneous material that produces TPA from PET by using a hydrolysis reaction. The majority of PET acid hydrolysis processes occur in the presence of homogeneous catalysts such as  $\rm H_2SO_4$ ,  $^{21}$  HNO $_3$ ,  $^{22}$  or HCl.  $^{23,24}$  Recently, a few recyclable systems capable of reacting PET by hydrolysis have been reported, but their experimental results in terms of conversion and selectivity remain quite low. For example, poly(4-styrenesulfonic acid) (PSSA)<sup>25</sup> is a catalyst that dissolves in water and can be recovered after the reaction by evaporating the filtrate solution. PSSA shows activity similar to that of H<sub>2</sub>SO<sub>4</sub>, but at much shorter reaction times. For instance, more than 90% PET conversion and TPA yield were achieved in the presence of PPSA in shorter times than when using the same concentration of H2SO4 was used However, such a system still requires the use of concentrated acid solutions that are corrosive and demand a subsequent neutralization step after the reaction.<sup>25</sup> There are also acid heterogeneous catalysts reported in the literature for the hydrolysis process, but these require particular conditions, such as  $SO_4^{2-}/TiO_2^{26}$  or  $WO_x/TiO_2^{27}$  in supercritical  $CO_2$  or  $H^+$ -ZSM-5 under microwaved irradiation.<sup>28</sup> A low stability was observed for solids including  $SO_4^{2-}/TiO_2$ , in which the leaching of sulfonated groups during hydrolysis was observed.<sup>26</sup> Therefore, finding a catalyst with strong and stable acid sites that could properly accommodate the diffusion of large molecules such as PET monomers would be a good first

step in developing a robust catalyst for PET depolymerization by a hydrolysis route.

Recently discovered in 2011, $^{29-31}$  MXenes are a novel family of two-dimensional (2D) metal carbide—nitride materials that have rapidly become a rising star in the scientific community because of their multiple and versatile applications. Typically, MXenes are synthesized from their parent MAX phase (M: an early transition metal; A, group IIIA or IVA elements; X: C and/or N; and n=1,2,3). The A layer (group IIIA or IVA elements like Si, Al, Sn, etc.) is selectively etched without breaking the M–X bonds, which are stronger compared with the M–A bonds from the MAX phase. The resulting MXene 2D sheets have the general formula of  $M_{n+1}X_nT_x$ , where  $T_x$  stands for surface terminations such as fluorine (–F), oxygen (–O), and hydroxyl (–OH). Due to their large surface areas and the significant impact of functional groups on their surfaces, MXenes are well-suited for use in catalytic processes.

Thus, a potentially useful approach to control MXenes' catalytic activity is to tune their surface chemistries. Therefore, to successfully address this challenge, herein we developed solid acid catalysts by modifying the MXene surfaces with acid moieties to obtain  $-SO_3H$ -modified MXenes (Scheme 1) capable of depolymerizing PET by hydrolysis. The important insight is that the 2D structure of MXene will provide more accessible  $-SO_3H$  groups for the bulky reactants and products (see Scheme 1).

Specifically, we studied the influence of reaction temperatures, catalyst loading, catalyst acidities, and reaction times on PET conversion and the TPA yield over acid-modified MXene catalysts.

#### **■ EXPERIMENTAL SECTION**

**Material Preparation.** *Synthesis of MAX Phase, Ti*<sub>3</sub>*AlC*<sub>2</sub> *Powder.* TiC, (Alfa Aesar, 99.5% 2 μm), Ti (Alfa Aesar, 99.5%, 325 mesh), and Al (Alfa Aesar, 99.5%, 325 mesh) were the commercial materials used in this step. The synthesis of Ti<sub>3</sub>AlC<sub>2</sub> powders involved combining of TiC, Al, and Ti powders at a molar ratio of 2:1.05:1, respectively. The powders of mixed composition underwent a ball milling process for 24 h at a rotational speed of 70 rpm utilizing zirconia balls. Subsequently, the powders were introduced into an alumina (Al<sub>2</sub>O<sub>3</sub>) tube furnace and heated to 1500 °C for a duration of 3 h while maintaining a continuous flow of argon (Ar) gas. The rates of heating and cooling were established at 5 °C per minute. The obtained porous blocks were ground into a fine powder with a drill press. The milled powders underwent a sieving process, using a ~400 mesh sieve, to obtain the Ti<sub>3</sub>AlC<sub>2</sub> powder with a particle size <38 μm.

Synthesis of  $Ti_3C_2T_x$  Powders. Aluminum removal from  $Ti_3AlC_2$  (MAX phase) to obtain  $Ti_3C_2T_x$  (MXene) was achieved by an etching process using a solution of LiF and HCl to generate HF in situ.<sup>34</sup> This step was carried out in Berzelius beakers made of poly-(tetrafluoroethylene), a thermoplastic and inert fluorinated polymer.

The procedure is the following: 0.66 g of LiF was added to 17 mL of 3 M HCl solution under continuous stirring until the salt was completely dissolved, and then 1 g of  ${\rm Ti}_3{\rm AlC}_2$  was added progressively in small amounts. The mixture was then stirred for 48 h at 50 °C before washing the resulting material 5 times with deionized water and separated by centrifugation (3500 rpm × 10 min for each washing cycle) until the pH of the supernatant was around 6–7. The final product  $({\rm Ti}_3{\rm C}_2{\rm T}_x)$ , in the form of a colloidal suspension, was vacuum filtered using a nylon membrane and dried under vacuum at 60 °C for 24 h.

 $SO_3H$  Modification of MXene. For the grafting of sulfonic groups to the  ${\rm Ti}_3{\rm C}_2{\rm T}_x$  surfaces, an aryl diazonium salt, obtained from sulfanilic acid was employed. The aryl diazonium salt of sulfanilic acid was prepared in situ<sup>35</sup> by reacting sulfanilic acid (0.1 g), sodium nitrite (0.375 g), anhydrous sodium carbonate (0.03 g), and a solution of HCl (2 mL of 37% HCl in 2 mL of H<sub>2</sub>O) (see Scheme 2).

## Scheme 2. Reaction Leading to Aryl Diazonium Salt Formation

sulfanilic acid (aqueous zwitterionic form) aryl diazonium salt

The procedure was as follows:  $Na_2CO_3$  was dissolved in water, and then sulfanilic acid was added, and the mixture was stirred until it completely dissolved at room temperature (RT). Then  $NaNO_2$  was added while being stirred to obtain a homogeneous solution. In a separate vial, we mixed 2 mL of cold water with 2 mL of HCl (37%). This solution was then added dropwise to the mixed solution with continuous stirring. Note the mixture must be kept at 0-5 °C to avoid decomposition of the aryl diazonium salt.  $Ti_3C_2T_x$  was added to the reaction mixture after being previously dispersed in distilled water (0.05 g of  $Ti_3C_2T_x$  in 5 mL of  $H_2O$ ). The resulting mixture was stirred in an ice bath (0-5 °C) for  $\sim$ 5 h. The final solution was cold filtered using a vacuum filtration system, washed with bidistilled water, and dried at 40 °C under vacuum. The material obtained is henceforth labeled  $Ti_3C_2T_x-SO_3H-1$  to indicate the 0.1 g of sulfanilic

Using the same protocol, two other batches of (a)  ${\rm Ti_3C_2T_x-SO_3H-3}$  (using 0.3 g of sulfanilic acid) and (b)  ${\rm Ti_3C_2T_x-SO_3H-5}$  (using 0.5 g of sulfanilic acid) were synthesized in which the MXene amount was kept constant (0.05 g), but the amounts of reagents needed to obtain the aryldiazonium salt were changed as follows: (a) sulfanilic acid (0.3 g), sodium nitrite (0.1125 g), anhydrous sodium carbonate (0.09 g), HCl solution (6 mL 37% HCl in 2 mL  ${\rm H_2O}$ ); (b) sulfanilic acid (0.5 g), NaNO<sub>2</sub> (0.1875 g), anhydrous Na<sub>2</sub>CO<sub>3</sub> (0.15 g), HCl solution (10 mL 37% HCl in 10 mL  ${\rm H_2O}$ ) were mixed. The reaction mixtures were kept under continuous stirring on a magnetic stirrer in an ice bath (0–5 °C) for ~5 h. The final solutions were cold filtered using a vacuum filtration system, washed with bidistilled water, and ovendried at 40 °C under vacuum.

**Material Characterization.** Scanning Electron Microscopy. The studied samples were imaged in scanning electron microscope (SEM) (Zeiss EVO 50 XVP) operated at an accelerating voltage of 20 kV and a LaB<sub>6</sub> filament as the electron source.

Transmission Electron Microscopy. The samples were also imaged in a transmission electron microscope (TEM) (JEOL 2100) with high-resolution and elemental X-ray mapping capabilities. The samples were prepared by the standard method for powders: (i) obtaining a suspension in ethanol of the desired sample, and (ii) dropping it onto a Cu grid with a carbon membrane. Conventional

TEM imaging, high-resolution TEM imaging, electron diffraction, and X-ray elemental mappings were performed.

X-ray Diffraction. Crystal structure analyses of the obtained materials was determined by powder X-ray diffraction (XRD) using a diffractometer (Bruker D8 ADVANCE) with Cu Kα radiation ( $\lambda$  = 1.5418 Å). Samples were analyzed in a symmetric geometry (Bragg–Brentano) in the angular range  $2\theta$  = 5–90°, using a step size of 0.02° and a time per step of 0.5 s. The interplanar d-spacings were calculated using Bragg's law. Additionally, small-angle X-ray analysis was performed on another diffractometer (Rigaku SmartLab 3 kW), also with Cu Kα radiation, using the following parameters:  $2\theta$  = 1.2–18° angular range, using a step size of 0.02 and a scan rate of 0.15°/min.

Raman Spectroscopy. All Raman spectra were recorded at room temperature, RT, in the 100–2000 cm<sup>-1</sup> range on a Raman spectrometer (LabRAM HR Evolution, HORIBA Jobin Yvon) equipped with a He–Ne laser (633 nm) and a charge-coupled device Peltier-cooled detector. To achieve high spectral resolution a grating of 1800 lines per millimeter was used. All spectra were recorded by averaging 5 accumulations, each of 30 s of laser exposure (ND filter of 25%).

*X-ray Photoelectron Spectroscopy.* The chemical state of the elements subjected to etching and sulfonation and subsequently used in catalytic PET depolymerization reactions was revealed by a X-ray photoelectron spectroscopy (XPS) spectrometer (Kratos Analytical Axis Ultra DLD) equipped with a monochromatic Al K $\alpha$  (1486.6 eV) radiation source. The measurements were conducted under the following conditions: a pressure of 1×10–8 Pa and a power of 144 W (12 kV×12 mA). To mitigate charging effects, a charge neutralizer was utilized. Calibration was carried out at the C 1s line (BE = 284.6 eV, C–C bond) of the adsorbed hydrocarbon on the surface of each sample. The experimental results were analyzed using the XPST plugin in Igor Pro8 from Wavemetrics.

ATR-FTIR. The FTIR spectroscopy measurements were performed in a spectrometer (PerkinElmer Spectrum BX II apparatus PerkinElmer Corporation, Waltham, MA, USA) in attenuated total reflectance (ATR) mode, with a diamond-zinc selenide crystal, 1.8 mm diameter. The spectra were obtained in the 500–4000 cm<sup>-1</sup> wavenumber range, with a resolution of 4 cm<sup>-1</sup> and 32 scans per acquisition.

Thermogravimetric Analysis. Thermogravimetric analysis (TGA) was performed by using a Themys One 1150 TGA thermal analyzer. Samples were heated up to 700  $^{\circ}$ C at a heating rate of 10  $^{\circ}$ C min<sup>-1</sup> in nitrogen (N<sub>2</sub>) flow of 20 mL min<sup>-1</sup>.

Temperature-Programmed Desorption of NH<sub>3</sub> (NH<sub>3</sub>-TDP). TPD profiles were measured by using a chemisorption apparatus (TRIFLEX, Micromeritics) equipped with a thermoconductivity detector. First, the samples were heated to 150 °C in helium (He) for 2 h and then cooled down to 100 °C. Then, 5 vol % NH<sub>3</sub> in He (15 mL min<sup>-1</sup>) was passed over the sample for 30 min. The physiosorbed NH<sub>3</sub> was removed using He (25 mL min<sup>-1</sup>, 100 °C for 1 h). The desorption of NH<sub>3</sub> was recorded by heating the sample up to 500 °C at a rate of 10 °C min<sup>-1</sup>, in a constant He flow rate of 25 mL min<sup>-1</sup>.

**Catalytic Reaction.** PET flakes  $(3 \times 2 \text{ mm}^2)$  were obtained by cutting small pieces of different PET sources and colors, bottles (white and green) and T-shirts shown in Figure S1 in Supporting Information. They were washed in hot water at 80 °C and dried for 2 h at 105 °C in an oven. If not mentioned otherwise, the following amounts of reactants were used for the catalytic reactions: 0.1 g PET flakes and 0.02 g catalyst (SO<sub>3</sub>H-modified MXenes) in 10 mL water for different reaction times that ranged between 2 and 24 h. The reactants were placed in a stainless-steel batch reactor equipped with a magnetic stirrer and a manometer. The reactor was purged with N2 to replace the air and to increase the internal pressure to 10 bar to maintain the water in a liquid state at the reaction temperatures (160-180 °C). The reactions were conducted in triplicate to ensure accuracy and reliability. The acquired results exhibited a maximum variability of 5% and were therefore considered consistent. The data reported in this study represent the average values obtained.

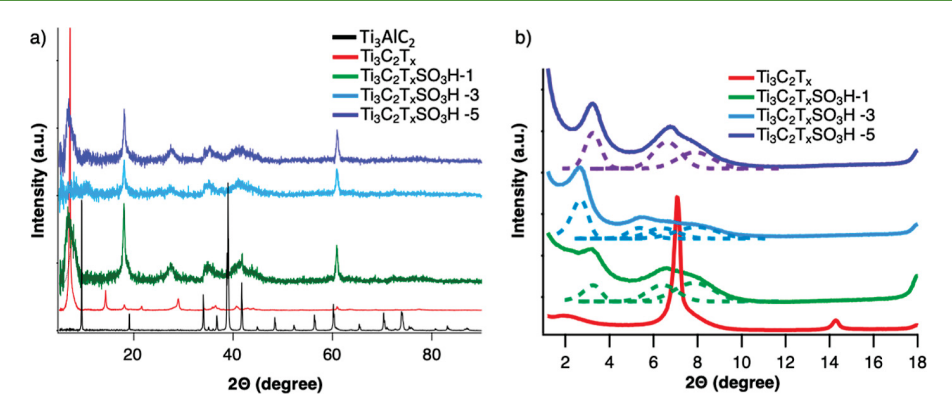


Figure 1. (a) Powder XRD diagrams and (b) low-angle XRD patterns of  $Ti_3C_2T_x$ ,  $Ti_3C_2T_x$ - $SO_3H$ -1,  $Ti_3C_2T_x$ - $SO_3H$ -3, and  $Ti_3C_2T_x$ - $SO_3H$ -5 samples. Designations and patterns are color coded.

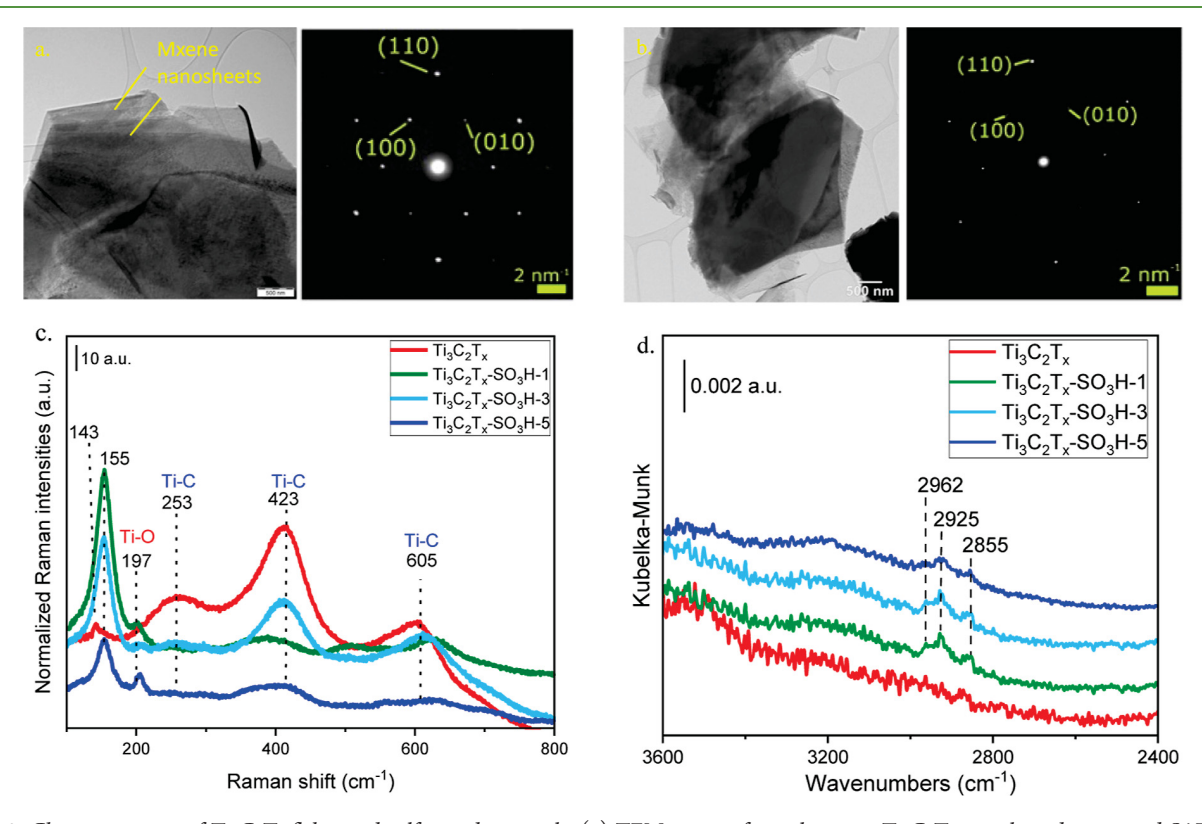


Figure 2. Characterization of  $Ti_3C_2T_x$  flakes and sulfonated materials. (a) TEM image of nanolayers in  $Ti_3C_2T_x$  sample and associated SAED, (b) TEM image of  $Ti_3C_2T_x$ -SO<sub>3</sub>H-1 nanolayers and associated SAED, (c) Raman spectra, and (d) ATR spectra of pristine and sulfonated  $Ti_3C_2T_x$  materials. Labels and curves are color coded for clarity.

**Leaching Tests.** In order to confirm the leaching of the sulfonic acid group during the depolymerization reaction, we conducted the following test: after reaction (0.1 g PET, 0.6 g  ${\rm Ti_3C_2T_x\text{-}SO_3H\text{-}5}$ , 10 mL  ${\rm H_2O}$ , 180 °C, 10 bar  ${\rm N_2}$ ), we filtered the reaction mixture and added the filtrate back into the reactor with an equal amount of PET (0.1 g) without catalyst. We then repeated the reaction and assessed its activity. No TPA was found throughout the response tests.

Processing of the Reaction Products after PET Hydrolysis. After the reaction time was completed, the reactor was cooled at RT and depressurized, and then the solid product (containing the catalyst, unprocessed PET and TPA obtained in the reactor after the catalytic reaction) was filtered to separate it from the EG, obtained as a byproduct in the liquid phase. The as-produced TPA was separated from the catalyst by the following method: the solid residue was washed with 1 M NaOH solution to form a soluble TPA—sodium salt and recover it in the liquid phase, and then the catalyst was dried in vacuum conditions. The TPA—Na dissolved in the NaOH solution

was recovered from the filtrate and recrystallized by adding twice the equivalent amount of a 2 M HCl solution. The white precipitate obtained by recrystallization was filtered, dried, and weighed (Figure S2d). The formation of TPA was confirmed by <sup>1</sup>H NMR and <sup>13</sup>C (see Figure S2).

PET conversion and product yields were calculated using the following equations

conversion PET = 
$$\{(W_{\rm PET,0}-W_{\rm PET,f})/W_{\rm PET,0}\} \times 100$$
  
yield TPA =  $\{W_{\rm TPA}/{\rm theoretical}\ W_{\rm TPA}\} \times 100$ 

where  $W_{\mathrm{PET},0}$  = initial mass of PET;  $W_{\mathrm{PET},f}$  = PET mass after reaction;  $W_{\mathrm{TPA}}$  = TPA mass obtained by hydrolysis, and theoretical  $W_{\mathrm{TPA}}$  = theoretical mass of TPA from initial PET, all in grams.

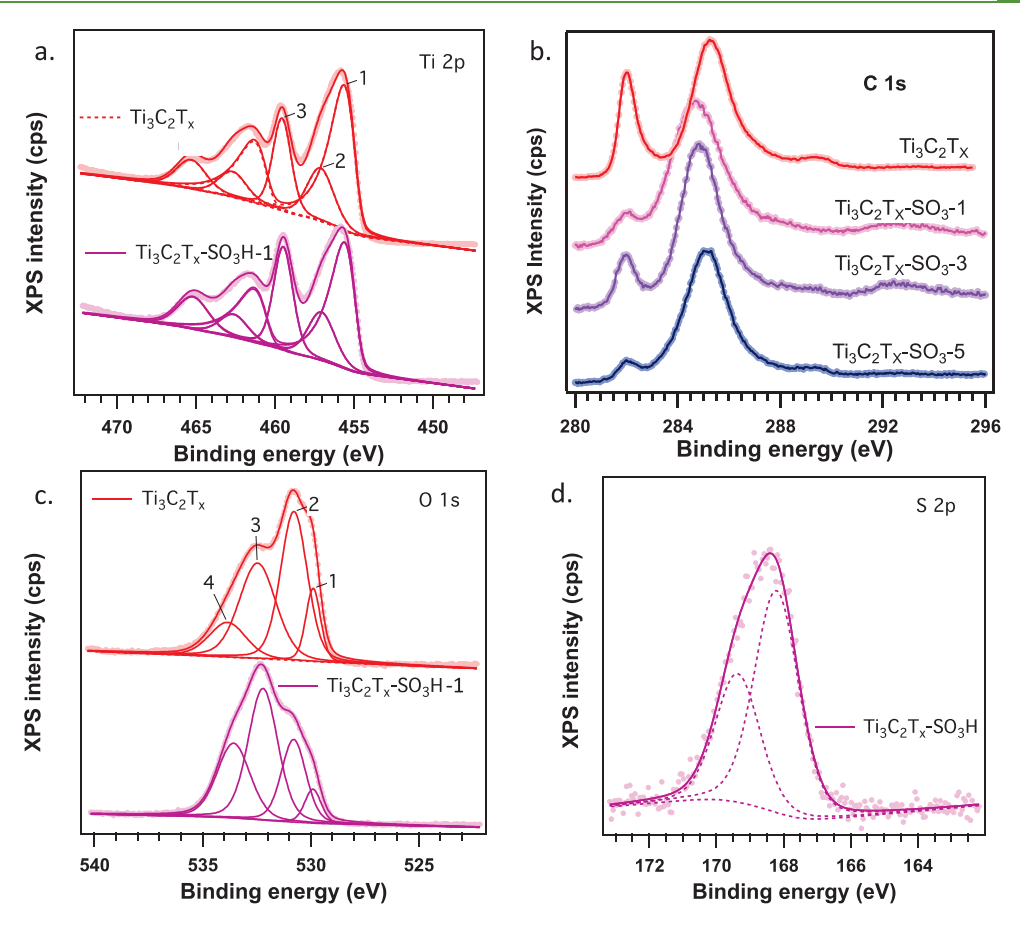


Figure 3. Comparison between  $Ti_3C_2T_x$  and  $Ti_3C_2T_x$ — $SO_3H$ -1 after surface modification by the reaction with sulfanilic acid. Core level spectra of (a)  $Ti_3P_1$  (b)  $Ci_3P_2$  (c)  $Ci_3P_3$  (d)  $Ci_3P_3$  (e)  $Ci_3P_3$  (e)  $Ci_3P_3$  (f)  $Ci_3P_3$ 

#### ■ RESULTS AND DISCUSSION

Physicochemical Characterization. From the powder XRD patterns (Figure 1a), it can be observed, for Ti<sub>3</sub>C<sub>2</sub>T<sub>x</sub> sample, the disappearance of the diffraction peak corresponding to the diffraction plane (104) at  $2\theta \sim 39^{\circ}$ , which is characteristic for Ti<sub>3</sub>AlC<sub>2</sub>. At the same time, the MAX phase peak corresponding to the (002) basal plane peak at  $2\theta \sim 9.5^{\circ}$ shifts to lower  $2\theta$  values after the etching process, i.e., to  $\sim 7.3^{\circ}$ , and its intensity increases significantly, confirming that the layered 2D structure is obtained, and the interlayer distance is modified. The interlayer distance, d, calculated for Ti<sub>3</sub>AlC<sub>2</sub> and  $Ti_3C_2T_x$  was 9.3 and 12.0 Å, respectively. These results are typical and are a key feature of the MAX to MXene transformation.<sup>36</sup> Comparing the sulfonated Ti<sub>3</sub>C<sub>2</sub>T<sub>x</sub>-SO<sub>3</sub>Hx materials' XRD patterns to unmodified MXene (Figure 1b), a further clear shift of the low angle peaks to lower  $2\theta$  angles occurs. This shift indicates an increased d-spacing between the MXene layers, suggesting the successful intercalation of aryl sulfonated groups between the MXene layers. For instance, the diffraction peak at  $2\theta$  of  $7^{\circ}$  is much wider and can be fitted with two peaks that correspond one to 12 Å distance of the 002 plane and a second one to an increased interplane distance of 15 Å, demonstrating the intercalation of aryl-sulfonic groups between the MXene layers. The shift of the line characteristic to (002) plan is obvious for  $Ti_3C_2T_x-SO_3H-x$  (x = 1, 3, 5), and moreover, a peak appears at  $2\theta$  around  $3^{\circ}$ , indicating a clear increase of d to 28 Å (Figure 1b). SEM micrographs of the various powders are shown in Figure S3, and disclose no obvious signs of destruction/deformation of the layered

structure of the material. Additionally, SEM–EDX data (see Table S1) reveal that after the etching process the Al layer is selectively removed from the MAX phase precursor. The layered structure arranged in very thin sheets appears to be maintained for the sulfonated  ${\rm Ti_3C_2T_x}$ –SO<sub>3</sub>H-1 material (Figures S3b,c), with no obvious signs of distortion. Compared to  ${\rm Ti_3C_2T_x}$ , the presence of –SO<sub>3</sub>H groups in  ${\rm Ti_3C_2T_x}$ –SO<sub>3</sub>H-x increases the interlayer spacing through the intercalation of functional groups; this is also confirmed by TEM and XRD analysis.

TEM data presented in Figures 2a and S4, in agreement with SEM analysis, revealed that the etching of Ti<sub>3</sub>AlC<sub>2</sub> was successful. In both samples (Ti<sub>3</sub>AlC<sub>2</sub> and Ti<sub>3</sub>C<sub>2</sub>T<sub>x</sub>), crystalline zones can be observed, with 2D overlapping sheets, with the particularity that for the Ti<sub>3</sub>C<sub>2</sub>T<sub>x</sub> sample small areas (about 100 nm) with an elongated appearance were also spotted. The diffraction signal of 2D zones is obtained for an orientation of the system along the c-axis and shows hexagonal symmetry (Figure 2a). The structural difference between Ti<sub>3</sub>AlC<sub>2</sub> and  $Ti_3C_2T_r$  is minor, but in conjunction with the lack of Al as well as the morphology of the 2D sheets, the association with the MXene system is much more likely. After  $Ti_3C_2T_x$  sulfonation, the high-resolution image illustrates a more evident appearance of the 2D sheets specific to the MXene system (Figure 2b). Again, diffraction is associated with the Ti<sub>3</sub>C<sub>2</sub> phase as is depicted in Figures 2b and S4. Selected area diffraction (SAD) patterns in the TEM confirm that the 2D structure remains intact.

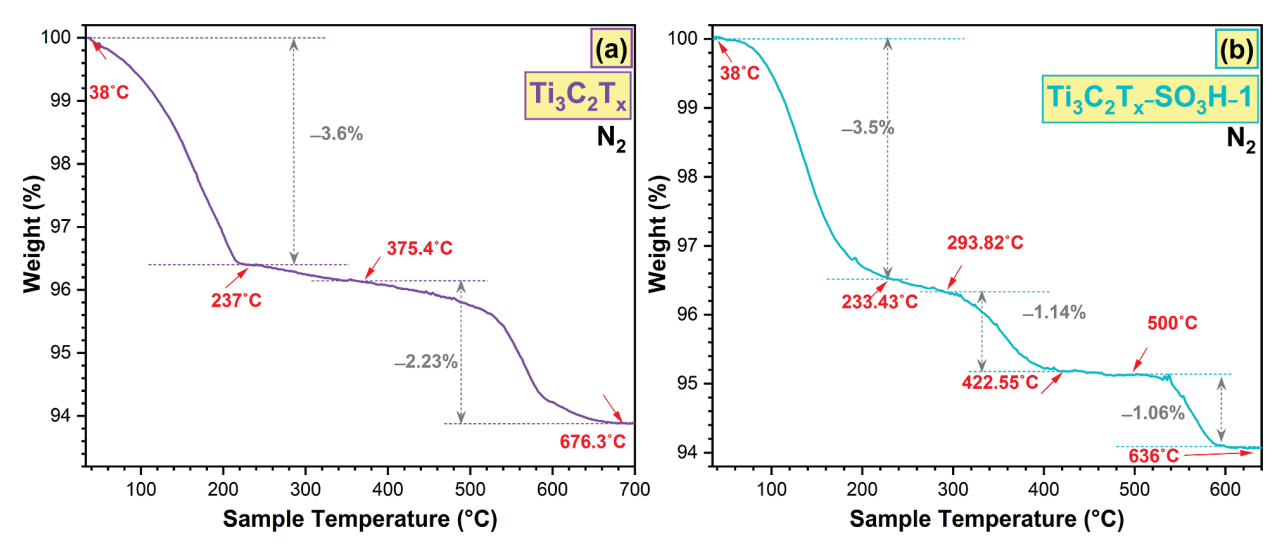


Figure 4. TGA profiles of (a)  $Ti_3C_2T_x$  and (b)  $Ti_3C_2T_x$ -SO<sub>3</sub>H-1.

The elemental maps in the SEM (Figure S5) as well as the EDX quantification results confirm the presence of Ti and C and the absence of Al (Figure S5 and Table S1). Furthermore, the detection of S in the sulfonated materials suggests that the aryl diazonium salt of the sulfanilic acid is present. Additionally, as presented in Table S1, it is evident that the quantity of sulfonated groups increased as the initial amounts of sulfanilic acid increased.

More evidence for the grafting of the sulfonic acid groups can be found in the Raman and ATR–FTIR spectra, as shown in Figure 2c,d, respectively. From the Raman spectra, it is reasonable to conclude that the  ${\rm Ti_3C_2T_x}$  structure was not affected by the sulfonation process (Figure 2c), which confirms both the XRD and TEM results. Thus, all samples show specific  ${\rm Ti_3C_2T_x}$  Raman active modes of two out-of-plane  ${\rm A_{1g}}$  and one degenerate in-plane  ${\rm E_{1g}}$  vibrations located at 253, 423, and 605 cm<sup>-1</sup>, respectively. The Eg mode attributed to  ${\rm TiO_2}$  anatase and located in the case of fresh  ${\rm Ti_3C_2T_x}$  sample at 143 cm<sup>-1</sup> shifts to 155 cm<sup>-1</sup> for the sulfonated samples which could be due to the presence of S. Also, a new typical  ${\rm TiO_2}$  band located at 197 cm<sup>-1</sup> appears, which makes it reasonable to conclude that upon sulfonation process, the MXene surfaces start to slightly oxidize.

Moreover, during the sulfonation process the amount of amorphous carbon, presumably at the surface, increases as evidenced by the appearance of both D and G bands located at 1337 and 1550 cm<sup>-1</sup>, respectively (see Figure S6), most probably traceable to the aryl moieties from the sulfanilic acid structure. This is also sustained by the appearance of new bands located at 2855 and 2962 cm<sup>-1</sup> in ATR spectra (Figure 2d) that can be assigned to the aromatic C–H symmetric and asymmetric stretching vibrations, respectively, while the band located at 2925 cm<sup>-1</sup> can be allocated to the stretching vibration of hydroxyl groups on the sulfanilic acid groups (–S–OH).<sup>43</sup> This is a direct evidence that sulfonation was successfully performed.

Figure S7a plots the Al 2p high-resolution XPS spectra of  ${\rm Ti}_3{\rm AlC}_2$  (black) and  ${\rm Ti}_3{\rm C}_2{\rm T}_x$  (blue). The absence of an Al signal in the spectrum (Figure S7b) proves that Al was removed during the etching process, in agreement with the SEM–EDX data. The high-resolution Ti 2p and O 1s core spectra of  ${\rm Ti}_3{\rm AlC}_2$  (black) and  ${\rm Ti}_3{\rm C}_2{\rm T}_x$  (blue) are shown in

Figure S7c,d. Like in all previous  $Ti_3C_2T_x$  work, <sup>44</sup> the Ti 2p and O 1s envelopes are shifted to higher binding energies, BEs, indicating that the MAX to MXene conversion results in the oxidation of the former. The spectra of the O 1s after sulfonation are shown in Figure 3c and again indicate that sulfonation results in more surface oxidation. In the C 1s case (Figure S7d), the peak at 282 eV is more intense in the  $Ti_3AlC_2$  than  $Ti_3C_2T_x$ . Since the 282 eV peak is fundamental to identifying  $Ti_3C_2T_x$ . Since the 282 eV see it is still present, albeit with a reduced intensity, after sulfonation (Figure 3b).

Changes in the surface composition of the acid-modified MXene materials were also observed in XPS measurements (Figure 3). Comparing the Ti 2p, C 1s, and O 1s XPS energy level spectra of the  $Ti_3C_2T_x$  and  $Ti_3C_2T_x$ -SO<sub>3</sub>H-x samples (x= 1, 3, 5) a clear S signal is detected at 168.0 eV (specific to the SO<sub>3</sub> group). 45 The O 1s core level spectrum has been fitted in four components at 529.9, 530.7, 532.5, and 533.6 eV, which are attributed to -C-Ti-O, Ti-O, and -OH bonds, respectively. The component at higher binding energy can be attributed to adsorbed water. The increase of the component at 532.5 eV after sulfanilic acid modification can be correlated with the oxygen present in -SO<sub>3</sub>H. Also, after sulfonation, the Ti 2p high-resolution spectra show no important changes among components of Ti 2p, which can be found at 455.5, 457.1, and 459.5 eV, and correspond to Ti-C  $(2p_{3/2})$ , Ti-C-O  $(2p_{3/2})$ , and TiO<sub>2</sub>, respectively. The C 1s core level shows, after sulfonation, a surface with fewer components than the complex MXene surface (282.0, 285.8, 287.6, and 289.8 eV attributed to Ti-C, C-C, C-O, and C=O, respectively),46 thus evidencing the presence of an organic compound on the surface, with predominate peaks at energies corresponding to C-C, C-O, and C=O.

Comparing the MXene surface chemistries before and after the sulfonation process, it is clear that the ratios of the various elements change (Table S2). Thus, a general trend of increasing relative C content and decreasing Ti content can be observed, leading to the obvious conclusion that the surface-attached aryl sulfonic compound increases the carbon content at the surface of the sulfonated samples.

The thermal behavior of our samples was studied by TGA. Thermogravimetric measurements achieved in a  $N_2$  atmosphere of  $Ti_3C_2T_x$  and  $Ti_3C_2T_x$ – $SO_3H-1$  samples are presented

in Figure 4a and b, respectively. For Ti<sub>3</sub>C<sub>2</sub>T<sub>x</sub> (Figure 4a), 3 weight loss regimes can be identified. The first (38-232 °C, i.e.,  $\sim$ 3.6%) indicates the removal of absorbed water molecules and possibly some of the functional groups  $(T_x)$  from the surface.<sup>47</sup> The second regime is ~2.23%, observed between ~436 and ~669 °C, and is ascribed to the annealing of  $Ti_3C_2T_r$  with the formation of small islands of  $TiO_2$ nanocrystals and amorphous carbon on the (2D) Ti<sub>3</sub>C<sub>2</sub>T<sub>r</sub> surface. In the  $Ti_3C_2T_r-SO_3H-1$  case, decomposition can be divided into three regions (Figure 4b). The first is a weight loss of ~3.5% from 38 to 229 °C of the water adsorbed on the surface and possibly some of the functional groups. The second, a slight weight reduction (~1.14%) occurring around 292-419 °C belongs, most probably, to the thermal decomposition of the sulfonic acid groups.<sup>35</sup> Another small weight loss (~1.06%) was found between 509 and 607 °C, which might be due to the loss of the benzene ring.<sup>35</sup> The TGA profile from Figure 4b indicates the successful sulfonation of the Ti<sub>3</sub>C<sub>2</sub>T<sub>x</sub> surface and also reveals that the MXene-SO<sub>3</sub>H-1 sample is stable up to 300 °C.

The acid properties of the modified MXene-based materials, in terms of the number of acid sites together with their strengths, were investigated by the  $TPD-NH_3$ . The results are listed in Table 1. As expected, the total amount of acid sites is

Table 1. Amount and Types of Acid Sites (µmol/g) Present in Ti<sub>3</sub>C<sub>2</sub>T<sub>x</sub>-SO<sub>3</sub>H According to TPD-NH<sub>3</sub>

acidity	$Ti_3C_2T_x$ -SO <sub>3</sub> -1 $(\mu \text{mol/g})$	$Ti_3C_2T_x-SO_3-3$ $(\mu mol/g)$	$Ti_3C_2T_x$ -SO <sub>3</sub> -5 $(\mu mol/g)$
weak	964	734	2841
medium	644	1452	704
strong			77
total	1608	2186	3622

directly proportional to the number of sulfonated groups present on the MXene surfaces. The NH<sub>3</sub>-TPD profiles as a function of S loadings are compared in Figure 5. For the  $\rm Ti_3C_2T_x-SO_3H-1$  and  $\rm Ti_3C_2T_x-SO_3H-3$  samples, the profiles show that as the temperature increases from 30 to 500 °C, two broad NH<sub>3</sub> desorption peaks appear corresponding to weak acidity at a temperature of approximatively 90 °C and a medium acidity at around 340 °C. When we analyze the different types of acidic sites, we are essentially referring to variations in the strength of these  $-\rm SO_3H$  groups.

The material with the largest concentration of sulfonic acid groups on its surface,  ${\rm Ti_3C_2T_x}\text{-}{\rm SO_3H}\text{-}5$ , was characterized by two relatively large peaks at 90 and 372 °C (Figure 5), which are weaker in the other materials. It is thus reasonable to conclude that the strength of acidity increases as the  ${\rm SO_3-H}$  content increases, most probably due to hydrogen bond formation between these functional groups. In other words, as Table 1 proves, the sample with the highest concentration of sulfonic groups possesses the strongest types of acid sites and the highest amount of acid groups. It is worth noting that the strength of sulfonic acid varies depending on factors such as the quantity of sulfonic acids loaded onto the surface and changes in the surrounding environment.

**Catalytic Reactions.** The catalytic activity of  ${\rm Ti_3C_2T_x}$ –  ${\rm SO_3H}$  materials was evaluated in PET hydrolysis by studying the main influencing factors. The catalytic results are summarized in Tables 2 and S3. Blank experiments, i.e., in the absence of the catalyst, were performed for 24 h at different

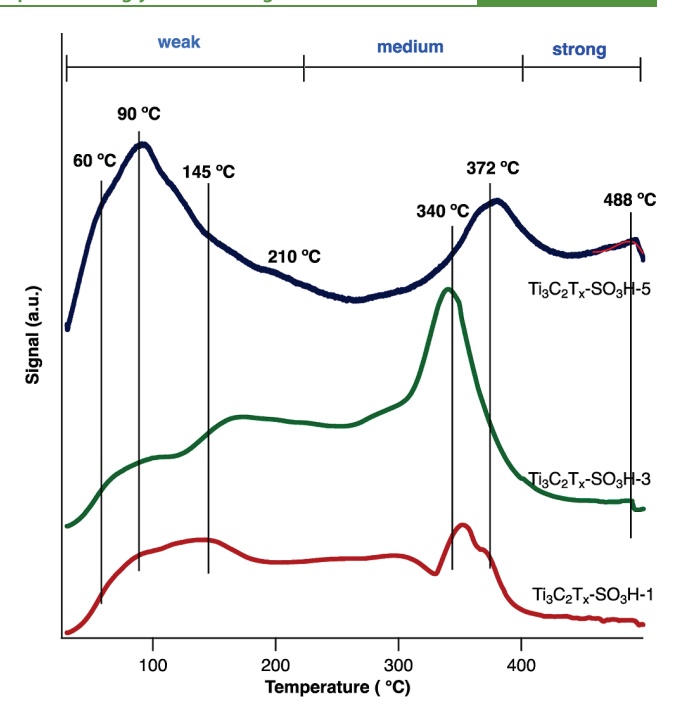


**Figure 5.** NH<sub>3</sub>-TPD curves of  $Ti_3C_2$ -SO<sub>3</sub>H-1,  $Ti_3C_2$ -SO<sub>3</sub>H-3, and  $Ti_3C_2$ -SO<sub>3</sub>H-5 samples indicated on plot.

Table 2. Catalytic Results of PET Hydrolysis Using Materials Synthesized Herein<sup>a</sup>

entry	catalyst	temperature ( $^{\circ}$ C)	TPA yield (%)
1	$\mathrm{Ti}_{3}\mathrm{C}_{2}\mathrm{T}_{x}$	180	0
2	$Ti_3C_2T_x$ -SO <sub>3</sub> H-1	180	56
3	$Ti_3C_2T_x$ -SO <sub>3</sub> H-3	180	66
4	$Ti_3C_2T_x$ -SO <sub>3</sub> H-5	180	72
5	$Ti_3C_2T_x$ -SO <sub>3</sub> H-5	170	44
6	$Ti_3C_2T_x$ -SO <sub>3</sub> H-5	160	0
7	$Ti_3C_2T_x$ - $SO_3H-5^{(i)}$	180	55
8	$Ti_3C_2T_x$ - $SO_3H-5^{(ii)}$	180	99

"Reaction conditions: stainless-steel batch reactor equipped with a magnetic stirrer and a manometer, 0.1 g PET flakes from a white bottle, 0.04 g catalyst in 10 mL water, 24 h; TPA product confirmed by <sup>1</sup>H NMR and <sup>13</sup>C NMR; (i) 0.02 g catalysts; (ii) 0.06 g catalyst.

temperatures (160, 170, and 180  $^{\circ}$ C) to ensure that no reaction occurs under the specific reaction conditions used. No conversion was observed for these tests. Another way to provide better control over the accuracy of the catalytic results was to use the as-synthesized MXene as a catalyst. Thus, it was confirmed that there were no depolymerization products in this case, in our specific reaction conditions (Table 2, entry 1).

As expected, the sulfonation of MXene increased the PET depolymerization conversion at 180 °C considerably (Table 2, entries 2–4). Comparing the three sulfonated MXenes, there is a direct correlation between the yields and the concentration of sulfonic groups present in the materials (Table 2, entries 2–4). According to TPD-NH<sub>3</sub>, a higher amount of a sulfonated group corresponds to a higher amount of acidic surface sites. From Table 1, one can see that the  $Ti_3C_2T_x$ – $SO_3H$ -5 samples have 1.25 times more acidic sites than  $Ti_3C_2T_x$ – $SO_3H$ -1. This again highlights the need for sulfonate groups on the surface.

Decreasing the temperature of depolymerization is an important step in the industrialization transfer process, considering that PET hydrolysis is an endothermic reaction;

therefore, we have verified the temperature effect onto the PET depolymerization using catalyst Ti<sub>3</sub>C<sub>2</sub>T<sub>x</sub>-SO<sub>3</sub>H-5. Lowering the temperature by 20 °C resulted in an inactive catalyst (Table 2, entry 6). At 170 °C, the TPA yield is 44% (Table 2, entry 5). The lack of activity of Ti<sub>3</sub>C<sub>2</sub>T<sub>x</sub>-SO<sub>3</sub>H-5 at 160 °C is most probably related to the PET depolymerization temperature dependency (Table 2, entry 6). While the PET depolymerization reaction occurs at 180 °C, in the presence of the catalyst, with a high yield, the lower temperature of 160 °C might not provide sufficient energy for the catalytic process to proceed effectively. The presence of Ti<sub>3</sub>C<sub>2</sub>T<sub>x</sub>-SO<sub>3</sub>H-5 changes the activation energy for PET depolymerization, requiring a minimum temperature threshold for catalytic activity to occur. Therefore, the inactivity at 160 °C suggests that the temperature might fall below this threshold, resulting in no catalytic effect.

Along the same lines, we investigated the reaction time's influence, at 180 °C, on TPA yield, starting with 0.04 g of  ${\rm Ti_3C_2T_x-SO_3H-1}$  catalyst. The results (Table S3) show that after 4 h, no conversion was observed; after 12 h, the conversion, at 3%, was also quite low. Increasing the reaction time to 24 h resulted in the highest TPA yield of 56%. These results suggest that the reaction has an induction time due to the high thermal stability of the PET, as already observed in other studies. <sup>49</sup> Again, not surprisingly, using a higher amount of catalyst increases the yield at 180 °C, as entries 4, 7, and 8 in Table 2 show.

Notably, by increasing the amount of catalyst, we obtained complete conversion with a yield of 99% to TPA starting with 0.06 g of  ${\rm Ti_3C_2T_x}{-}{\rm SO_3H}{-}5$  for 24 h at 180 °C. XRD patterns before and after the reaction (Figure S8) demonstrate that our catalysts are stable under the reaction conditions, confirming the results observed by TG-DTA, which predicted stability until 300 °C. Moreover, as data presented in Table S3,  ${\rm Ti_3C_2T_x}{-}{\rm SO_3H}{-}5$  was obtained after 3 cycles; in each case the TPA yield around 54%. This is important since it suggests that the same catalyst can be used multiple times.

Next, we examined the yields of PET samples obtained from different sources; clear and green bottles and T-shirts (see Figure S1). The data presented in Figure 6 show that the yields drop from 66% for clear bottles to 37% for the T-shirts and 31% for green bottles. The observed decrease in activity can be attributed to the presence of some possible PET additives that may dissolve in the reaction medium and possibly block the catalytic sites. These results indeed demonstrate that stabilizing polymeric additives present in these plastics can have significant negative impacts on the catalytic process and that the PETsource is thus important.

Figure 7 compares the results obtained herein with previous work on heterogeneous catalysts used for the hydrolysis of PET. As alluded to in the introduction, there are only a few studies on the truly heterogeneous catalytic hydrolysis of PET in the literature. Since in almost all reports, the heterogeneous catalysts are optimized to achieve high yields (98–99%), from the data we have, one can assume that the most important parameter to compare the catalysts is the reaction temperature of PET hydrolysis. Our best catalyst,  $Ti_3C_2T_x-SO_3H-5$ , presents a working temperature of  $180\,^{\circ}\text{C}$ ,  $40\,^{\circ}\text{C}$  lower than the pool of heterogeneous catalysts reported for this reaction (see Figure 7). Only one example,  $(SO_4)^{2-}/TiO_2$ ,  $^{50}$  is reported to be active at  $160\,^{\circ}\text{C}$ , but in supercritical conditions (pressure of  $150\,\text{bar}$ ), that are significantly harsher than ours. Moreover, low stability was observed for solids such as  $SO_4^{2-}/TiO_2$ , in

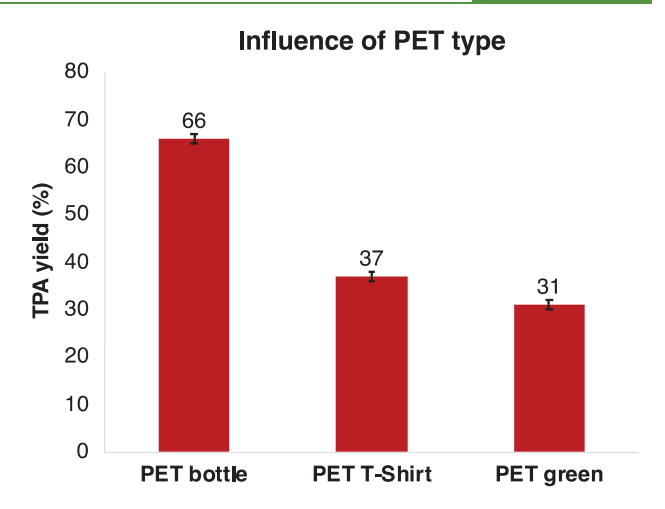


**Figure 6.** Comparison of the catalytic results at 180 °C of different PET materials using  $Ti_3C_2T_x$ – $SO_3H$ -3 catalyst, 0.1 g PET flakes, 0.04 g catalyst in 10 mL water, 24 h, 10 bar  $N_2$ . TPA product was confirmed by  $^1H$  NMR and  $^{13}C$  NMR. Error bars represent  $\pm 5\%$  standard deviation of TPA yield (all reactions were performed, at least in triplicate).

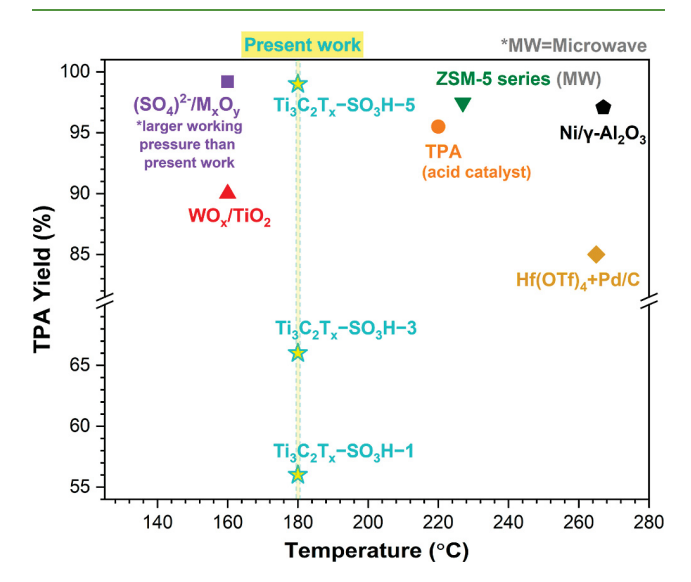


**Figure** 7. Comparison of literature data,  $HF(OTf)_4 + Pd/C_1^{13}(SO_4)^{2-}/TiO_2^{26}WO_x/TiO_2^{27}ZSM-5_1^{28}TPA_2^{51}$  and  $Ni/AlO_3^{52}$  on PET depolymerization by hydrolysis as a function of temperature.

which the leaching of sulfonated groups during hydrolysis was observed.

Our results suggest that the immobilization of acidic sites on MXene surfaces represent a good starting point for developing new solid acid catalysts. Thus, it was observed that an increase of acidic groups on the surface changes even the strength of the acidity existing in the material, most probably due to the interaction with the surface, which changes the geometry and the electronic structure of the active sites. Another important feature of our system is the flexibility of 2D MXene which can adapt quickly to the space between layers when bulky molecules are attached to the surface, thus increasing the accessibility of the PET and its bulky products to the active sites, which explains the high activities at lower temperatures.

#### CONCLUSIONS

In this study, a series of MXene 2D flakes modified with different concentrations of sulfonic acid groups,  $-SO_3H$ , were successfully prepared and characterized both structurally and morphologically. From the morphological point of view, a successful intercalation of the sulfonic acid groups was observed between the 2D  $Ti_3C_2T_x$  multilayers. The preservation of 2D structure together with the increase of distance between the multilayers are important features that allow the reactant and products to diffuse to and from the active sites more easily, thus increasing the activity. All the other characterization techniques employed demonstrate the true immobilization of the sulfonic acids between the MXene layers.

Using  ${\rm Ti_3C_2T_x}$  with the highest loading of sulfonic acid groups as catalyst, it is possible to depolymerize 99% of PET in water at 180 °C in 24 h. In agreement with the acidity measurements (TPD-NH<sub>3</sub>), indeed, the 2D  ${\rm Ti_3C_2T_x}$  modified with the highest amount of derived sulfonic acids contains the higher amount of acidity, and it is thus reasonable to conclude that the acidity is needed to perform the hydrolysis reaction. Through this study, we succeeded in obtaining acid-modified MXene catalysts that can break down PET at a temperature of 180 °C, that is 40 °C lower than other catalysts already used under comparable reaction conditions. Moreover, our catalysts are stable at least for 3 cycles. These findings suggest that both the acidity of the catalysts and the 2D features are important for the depolymerization of PET and, thus, acid-modified MXenes can be promoted as valuable catalysts for upcycling PET.

Scaling-up PET hydrolysis using a heterogeneous catalyst is feasible, but it also comes with challenges. It is crucial to maintain efficient reaction kinetics, handle mass transfer limitations, ensure good contact between the catalyst and the PET flakes, and evaluate the environmental impact during scaling-up. Although there are difficulties, tackling these aspects through research and optimization can facilitate the development of PET recycling operations on a wide scale.

### ■ ASSOCIATED CONTENT

#### Supporting Information

The Supporting Information is available free of charge at https://pubs.acs.org/doi/10.1021/acssuschemeng.4c01920.

Additional experimental details; materials; reaction scheme; <sup>1</sup>H NMR spectra for the reaction product; SEM micrographs of all the catalysts; TEM images and associated electron diffraction patterns; TEM elemental maps for different catalysts; elemental analysis according to EDX—both SEM and TEM; Raman spectra; XPS spectra; surface atomic ratios; catalytic results; and XRD patterns (PDF)

#### AUTHOR INFORMATION

#### **Corresponding Author**

Florentina Neaţu — National Institute of Materials Physics, Măgurele 077125, Romania; o orcid.org/0000-0002-7885-436X; Email: florentina.neatu@infim.ro

#### Authors

Iuliana M. Chirica – National Institute of Materials Physics, Măgurele 077125, Romania; Faculty of Physics, University of Bucharest, Măgurele 077125, Romania

- Anca G. Mirea National Institute of Materials Physics, Măgurele 077125, Romania
- Tudor Şuteu Faculty of Physics, University of Bucharest, Măgurele 077125, Romania
- Andrei Kuncser National Institute of Materials Physics, Măgurele 077125, Romania; o orcid.org/0000-0003-2841-5809
- Ştefan Neaţu National Institute of Materials Physics, Măgurele 077125, Romania; ⊚ orcid.org/0000-0002-2450-0291
- Mihaela Florea National Institute of Materials Physics, Măgurele 077125, Romania; orcid.org/0000-0002-6612-6090
- Michel W. Barsoum Department of Materials Science & Engineering, Drexel University, Philadelphia, Pennsylvania 19104, United States; Oorcid.org/0000-0001-7800-3517

Complete contact information is available at: https://pubs.acs.org/10.1021/acssuschemeng.4c01920

#### **Author Contributions**

The manuscript was written by all authors. IMC—catalysts preparation, catalytic reaction, partial characterization of the materials, and validation; TS—catalytic reaction; AGM—SEM analysis; AK—TEM analysis; SN—Raman analysis; MF—TPD-NH<sub>3</sub> and XPS validation and data interpretation; MWB—providing materials, visualization, writing, review, and editing; FN—conceptualization, writing, review and editing, and project administration. All authors have given approval to the final version of the manuscript.

#### Notes

The authors declare no competing financial interest.

#### ACKNOWLEDGMENTS

This work was supported by grants from the Ministry of Research, Innovation, and Digitization, CNCS—UEFISCDI, project number PN-III-P1-1.1-TE-2019-1969. Financial support from the Romanian Ministry of Research, Innovation, and Digitization through the Core Program 2023—2026 (contract PC3-PN23080303) is gratefully acknowledged. This work was partially funded by NSF (DMR-2211319).

#### REFERENCES

- (1) Shell Scenarios- SKY-Meeting the Goals of the Paris Agreement. 2024, http://www.shell.com/skyscenario (accessed Feb, 2024)
- (2) Lange, J.-P. Towards Circular Carbo-Chemicals the Metamorphosis of Petrochemicals. *Energy Environ. Sci.* **2021**, *14* (8), 4358–4376.
- (3) Hundertmark, T.; Mayer, M.; McNally, C.; Simons, T. J.; Witte, C. How Plastics-Waste Recycling Could Transform the Chemical Industry, McKinsey on Chemicals, 2018.
- (4) Vollmer, I.; Jenks, M. J. F.; Roelands, M. C. P.; White, R. J.; van Harmelen, T.; de Wild, P.; van der Laan, G. P.; Meirer, F.; Keurentjes, J. T. F.; Weckhuysen, B. M. Beyond Mechanical Recycling: Giving New Life to Plastic Waste. *Angew. Chem., Int. Ed.* **2020**, 59 (36), 15402–15423.
- (5) Chen, X.; Wang, Y.; Zhang, L. Recent Progress in the Chemical Upcycling of Plastic Wastes. *ChemSusChem* **2021**, *14* (19), 4137–4151.
- (6) Rahimi, A.; García, J. M. Chemical Recycling of Waste Plastics for New Materials Production. *Nat. Rev. Chem* **2017**, *1* (6), 46.
- (7) Filiciotto, L.; Rothenberg, G. Biodegradable Plastics: Standards, Policies, and Impacts. *ChemSusChem* **2021**, *14* (1), 56–72.
- (8) Vollmer, I.; Jenks, M. J. F.; Roelands, M. C. P.; White, R. J.; van Harmelen, T.; de Wild, P.; van der Laan, G. P.; Meirer, F.; Keurentjes,

- J. T. F.; Weckhuysen, B. M. Beyond Mechanical Recycling: Giving New Life to Plastic Waste. *Angew. Chem., Int. Ed.* **2020**, 59 (36), 15402–15423.
- (9) Nakaji, Y.; Tamura, M.; Miyaoka, S.; Kumagai, S.; Tanji, M.; Nakagawa, Y.; Yoshioka, T.; Tomishige, K. Low-Temperature Catalytic Upgrading of Waste Polyolefinic Plastics into Liquid Fuels and Waxes. *Appl. Catal., B* **2021**, *285*, 119805.
- (10) Celik, G.; Kennedy, R. M.; Hackler, R. A.; Ferrandon, M.; Tennakoon, A.; Patnaik, S.; LaPointe, A. M.; Ammal, S. C.; Heyden, A.; Perras, F. A.; Pruski, M.; Scott, S. L.; Poeppelmeier, K. R.; Sadow, A. D.; Delferro, M. Upcycling Single-Use Polyethylene into High-Quality Liquid Products. ACS Cent. Sci. 2019, 5 (11), 1795–1803.
- (11) Wang, L.; Li, G.; Cong, Y.; Wang, A.; Wang, X.; Zhang, T.; Li, N. Direct Synthesis of a Jet Fuel Range Dicycloalkane by the Aqueous Phase Hydrodeoxygenation of Polycarbonate. *Green Chem.* **2021**, 23 (10), 3693–3699.
- (12) Zhang, F.; Zeng, M.; Yappert, R. D.; Sun, J.; Lee, Y. H.; LaPointe, A. M.; Peters, B.; Abu-Omar, M. M.; Scott, S. L. Polyethylene Upcycling to Long-Chain Alkylaromatics by Tandem Hydrogenolysis/Aromatization. *Science* **2020**, *370* (6515), 437–441.
- (13) Kratish, Y.; Marks, T. J. Efficient Polyester Hydrogenolytic Deconstruction via Tandem Catalysis. *Angew. Chem., Int. Ed.* **2022**, *61* (9), No. e202112576.
- (14) Fukushima, K.; Lecuyer, J. M.; Wei, D. S.; Horn, H. W.; Jones, G. O.; Al-Megren, H. A.; Alabdulrahman, A. M.; Alsewailem, F. D.; McNeil, M. A.; Rice, J. E.; Hedrick, J. L. Advanced Chemical Recycling of Poly(Ethylene Terephthalate) through Organocatalytic Aminolysis. *Polym. Chem.* **2013**, *4* (5), 1610–1616.
- (15) Ghosal, K.; Sarkar, K. Poly(Ester Amide) Derived from Municipal Polyethylene Terephthalate Waste Guided Stem Cells for Osteogenesis. *New J. Chem.* **2019**, 43 (35), 14166–14178.
- (16) Nunes, B. F. S.; Oliveira, M. C.; Fernandes, A. C. Dioxomolybdenum Complex as an Efficient and Cheap Catalyst for the Reductive Depolymerization of Plastic Waste into Value-Added Compounds and Fuels. *Green Chem.* **2020**, 22 (8), 2419–2425.
- (17) Monsigny, L.; Berthet, J.-C.; Cantat, T. Depolymerization of Waste Plastics to Monomers and Chemicals Using a Hydrosilylation Strategy Facilitated by Brookhart's Iridium(III) Catalyst. ACS Sustain. Chem. Eng. 2018, 6 (8), 10481–10488.
- (18) Uekert, T.; Kasap, H.; Reisner, E. Photoreforming of Nonrecyclable Plastic Waste over a Carbon Nitride/Nickel Phosphide Catalyst. *J. Am. Chem. Soc.* **2019**, *141* (38), 15201–15210.
- (19) Uekert, T.; Kuehnel, M. F.; Wakerley, D. W.; Reisner, E. Plastic Waste as a Feedstock for Solar-Driven H2 Generation. *Energy Environ. Sci.* **2018**, *11* (10), 2853–2857.
- (20) Barnard, E.; Rubio Arias, J. J.; Thielemans, W. Chemolytic Depolymerisation of PET: A Review. *Green Chem.* **2021**, 23 (11), 3765–3789.
- (21) Yoshioka, T.; Motoki, T.; Okuwaki, A. Kinetics of Hydrolysis of Poly(Ethylene Terephthalate) Powder in Sulfuric Acid by a Modified Shrinking-Core Model. *Ind. Eng. Chem. Res.* **2001**, *40* (1), 75–79.
- (22) Yoshioka, T.; Okayama, N.; Okuwaki, A. Kinetics of Hydrolysis of PET Powder in Nitric Acid by a Modified Shrinking-Core Model. *Ind. Eng. Chem. Res.* **1998**, 37 (2), 336–340.
- (23) Ravens, D. A. S. The Chemical Reactivity of Poly(Ethylene Terephthalate): Heterogeneous Hvdrolysis by Hydrochloric Acid. *Polymer* **1960**, *1*, 375–383.
- (24) Davies, T.; Goldsmith, P. L.; Ravens, D. A. S.; Ward, I. M. THE KINETICS OF THE HYDROLYSIS OF POLYETHYLENE TEREPHTHALATE FILM. *J. Phys. Chem.* **1962**, *66* (1), 175–176.
- (25) Abedsoltan, H.; Omodolor, I. S.; Alba-Rubio, A. C.; Coleman, M. R. Poly (4-Styrenesulfonic Acid): A Recoverable and Reusable Catalyst for Acid Hydrolysis of Polyethylene Terephthalate. *Polymer* **2021**, 222, 123620.
- (26) Li, X. K.; Lu, H.; Guo, W. Z.; Cao, G. P.; Liu, H. L.; Shi, Y. H. Reaction Kinetics and Mechanism of Catalyzed Hydrolysis of Waste PET Using Solid Acid Catalyst in Supercritical CO2. *AIChE J.* **2015**, *61* (1), 200–214.

- (27) Guo, W. Z.; Lu, H.; Li, X. K.; Cao, G. P. Tungsten-Promoted Titania as Solid Acid for Catalytic Hydrolysis of Waste Bottle PET in Supercritical CO2. *RSC Adv.* **2016**, *6* (49), 43171–43184.
- (28) Kang, M. J.; Yu, H. J.; Jegal, J.; Kim, H. S.; Cha, H. G. Depolymerization of PET into Terephthalic Acid in Neutral Media Catalyzed by the ZSM-5 Acidic Catalyst. *Chem. Eng. J.* **2020**, 398, 125655.
- (29) Naguib, M.; Barsoum, M. W.; Gogotsi, Y. Ten Years of Progress in the Synthesis and Development of MXenes. *Adv. Mater.* **2021**, 33 (39), 2103393.
- (30) Kurtoglu, M.; Naguib, M.; Gogotsi, Y.; Barsoum, M. W. First Principles Study of Two-Dimensional Early Transition Metal Carbides. MRS Commun. 2012, 2, 133–137.
- (31) Naguib, M.; Kurtoglu, M.; Presser, V.; Lu, J.; Niu, J.; Heon, M.; Hultman, L.; Gogotsi, Y.; Barsoum, M. W. Two-Dimensional Nanocrystals Produced by Exfoliation of Ti<sub>3</sub>AlC<sub>2</sub>. *Adv. Mater.* **2011**, 23, 4248–4253.
- (32) Verger, L.; Natu, V.; Carey, M.; Barsoum, M. W. MXenes: An Introduction of Their Synthesis, Select Properties, and Applications. *Trends Chem.* **2019**, *1* (7), 656–669.
- (33) Chirica, I. M.; Mirea, A. G.; Neaţu, Ş.; Florea, M.; Barsoum, M. W.; Neaţu, F. Applications of MAX Phases and MXenes as Catalysts. *J. Mater. Chem. A* **2021**, *9* (35), 19589–19612.
- (34) Verger, L.; Xu, C.; Natu, V.; Cheng, H.-M.; Ren, W.; Barsoum, M. W. Overview of the Synthesis of MXenes and Other Ultrathin 2D Transition Metal Carbides and Nitrides. *Curr. Opin. Solid State Mater. Sci.* **2019**, 23 (3), 149–163.
- (35) Lei, Y.; Cui, Y.; Huang, Q.; Dou, J.; Gan, D.; Deng, F.; Liu, M.; Li, X.; Zhang, X.; Wei, Y. Facile Preparation of Sulfonic Groups Functionalized Mxenes for Efficient Removal of Methylene Blue. *Ceram. Int.* **2019**, 45, 17653–17661.
- (36) Naguib, M.; Kurtoglu, M.; Presser, V.; Lu, J.; Niu, J.; Heon, M.; Hultman, L.; Gogotsi, Y.; Barsoum, M. W. Two-Dimensional Nanocrystals Produced by Exfoliation of Ti3AlC2. *Adv. Mater.* **2011**, 23 (37), 4248–4253.
- (37) Syamsai, R.; Kollu, P.; Kwan Jeong, S.; Nirmala Grace, A. Synthesis and Properties of 2D-Titanium Carbide MXene Sheets towards Electrochemical Energy Storage Applications. *Ceram. Int.* **2017**, 43 (16), 13119–13126.
- (38) Sarycheva, A.; Gogotsi, Y. Raman Spectroscopy Analysis of the Structure and Surface Chemistry of Ti<sub>3</sub>C<sub>2</sub>T<sub>x</sub> MXene. *Chem. Mater.* **2020**, 32 (8), 3480–3488.
- (39) Cheng, L.; Chen, Q.; Li, J.; Liu, H. Boosting the Photocatalytic Activity of CdLa2S4 for Hydrogen Production Using Ti3C2MXene as a Co-Catalyst. *Appl. Catal., B* **2020**, *267*, 118379.
- (40) Spanier, J. E.; Gupta, S.; Amer, M.; Barsoum, M. W. Vibrational Behavior of the M N+ 1 a X N Phases from First-Order Raman Scattering (M= Ti, V, Cr, A= Si, X= C, N). *Phys. Rev. B: Condens. Matter Mater. Phys.* **2005**, *71*, 012103.
- (41) Arunmetha, S.; Dhineshbabu, N. R.; Kumar, A.; Jayavel, R. Preparation of Sulfur Doped TiO2 Nanoparticles from Rutile Sand and Their Performance Testing in Hybrid Solar Cells. *J. Mater. Sci.: Mater. Electron.* **2021**, 32 (24), 28382–28393.
- (42) Balachandran, U.; Eror, N. G. Raman Spectra of Titanium Dioxide. J. Solid State Chem. 1982, 42, 276–282.
- (43) Zhang, J.; Liu, Y.; Lv, Z.; Zhao, T.; Li, P.; Sun, Y.; Wang, J. Sulfonated Ti3C2Tx to Construct Proton Transfer Pathways in Polymer Electrolyte Membrane for Enhanced Conduction. *Solid State Ionics* **2017**, 310, 100–111.
- (44) Natu, V.; Benchakar, M.; Canaff, C.; Habrioux, A.; Célérier, S.; Barsoum, M. W. A Critical Analysis of the X-Ray Photoelectron Spectra of Ti3C2Tz MXenes. *Matter* **2021**, *4* (4), 1224–1251.
- (45) Shanthi, P. M.; Hanumantha, P. J.; Ramalinga, K.; Gattu, B.; Datta, M. K.; Kumta, P. N. Sulfonic Acid Based Complex Framework Materials (CFM): Nanostructured Polysulfide Immobilization Systems for Rechargeable Lithium-Sulfur Battery. *J. Electrochem. Soc.* **2019**, *166* (10), A1827–A1835.

- (46) Natu, V.; Benchakar, M.; Canaff, C.; Habrioux, A.; Célérier, S.; Barsoum, M. W. A Critical Analysis of the X-Ray Photoelectron Spectra of Ti3C2Tz MXenes. *Matter* **2021**, *4*, 1224–1251.
- (47) Han, M.; Yin, X.; Wu, H.; Hou, Z.; Song, C.; Li, X.; Zhang, L.; Cheng, L. Ti3C2MXenes with Modified Surface for High-Performance Electromagnetic Absorption and Shielding in the X-Band. ACS Appl. Mater. Interfaces 2016, 8 (32), 21011–21019.
- (48) Valadbeigi, Y. Acidity Enhancement of Sulfonic Acid Derivatives by Hydrogen Bond Networks. *Comput. Theor Chem.* **2021**, 1193, 113054.
- (49) Zhang, S.; Song, X.; Zhang, D.; Tian, Y. Kinetics of the Hydrolytic Depolymerization of Poly(Ethylene Terephthalate) under Microwave Irradiation. *Polym. J.* **2011**, 43 (10), 811–815.
- (50) Li, X. K.; Lu, H.; Guo, W. Z.; Cao, G. P.; Liu, H. L.; Shi, Y. H. Reaction Kinetics and Mechanism of Catalyzed Hydrolysis of Waste PET Using Solid Acid Catalyst in Supercritical CO2. *AIChE J.* **2015**, *61* (1), 200–214.
- (51) Yang, W.; Liu, R.; Li, C.; Song, Y.; Hu, C. Hydrolysis of Waste Polyethylene Terephthalate Catalyzed by Easily Recyclable Terephthalic Acid. *Waste Manage.* **2021**, *135*, 267–274.
- (52) Yan, M.; Yang, Y.; Chen, F.; Hantoko, D.; Pariatamby, A.; Kanchanatip, E. Development of Reusable Ni/ $\gamma$ -Al 2 O 3 Catalyst for Catalytic Hydrolysis of Waste PET Bottles into Terephthalic Acid. *Environ. Sci. Pollut. Res.* **2023**, *30*, 102560–102573.